Fibers and Polymers 2018, Vol.19, No.2, 357-363
DOI 10.1007/s12221-018-7888-6

ISSN 1229-9197 (print version)
ISSN 1875-0052 (electronic version)

Fabrication and Characterization of Graphene Enriched Polysulfon Amide Nanocomposites by Electrospinning System

Na Meng, Yuansheng Zheng*, and Binjie Xin*

School of Fashion Engineering, Shanghai University of Engineering Science, Shanghai 201620, P.R. China
(Received October 12, 2017; Revised December 25, 2017; Accepted December 27, 2017)

Abstract: In this paper, we report on the fabrication and characterization of poly(sulfone amide)/graphene (PSA/G) nonwoven based nanocomposite mat assembled via electrospinning technique. Different types of nanocomposite mats were electrospun by varying the weight percentage of graphene in the polymer solution. The surface morphologies, chemical structural, thermal, and electrical properties of the nanocomposites were evaluated systematically. The morphology of the PSA/G nanocomposites exhibited that mesh-like ultrafine nanofibers were densely aligned. Thermal stability and electrical properties of the PSA/G composites could be improved obviously with the addition of graphene. And the thickness uniformity of the nanocomposite mat was improved by using an electrospinning system. Our experimental results suggested that the PSA/G nanocomposites have potential to serve in many different applications, especially in the area of electronic components.

Keywords: Polysulfon amide/graphene nanocomposites, Electrospinning, Graphene, Electrical properties, Thermal properties

Introduction

Electrospinning is a versatile and straightforward method to produce the one-dimensional (1D, fibers) and two dimensional (2D, nonwoven fabric) structured materials at the nanoscale [1-6]. These electrospun nanofibrous materials have attracted increasing interests owing to their unique properties and numerous applications in areas of filtration media [7,8], life science [9,10], medicine [11,12] and electronic industries [13]. Scientists are trying to improve the physicochemical properties of the electrospun nanomaterials via composite method to make them more suitable in the field of nano science and technology [14-17]. Nanocomposites with various polymer matrices have shown excellent characteristics with small loading [18,19].

The two-dimensional monolayer carbon material graphene and its derivate has recently become a hot issue of scientific interest due to their remarkable properties [20-22]. The performance of the electrospun nanofiber or nanofibrous nonwoven could be enhanced with the addition of graphene. Therefore, graphene based polymer (polymer/graphene) nanocomposites have also attracted both academic and industrial interests in recent years. A large number of studies showed that polymer/graphene nanocomposites have superior mechanical, thermal, gas barrier, electrical and flame-retardant properties compared to the neat polymer [23-25]. It was also reported that the improvement in mechanical and electrical properties of graphene based polymer nanocomposites are much better in comparison to that of clay or other carbon filler-based polymer nanocomposites [26-29].

Recently, functionalized graphene-polymer nanocomposite is prepared with some polymers such as polystyrene, polyvinyl acetate, polyvinyl alcohol (PVA), and poly(methyl methacrylate) [30,31]. Poly(sulfone amide) (PSA), is one of the spinnable polymer known for their excellent thermal properties such as heat resistance, flame retardant, thermal stability and etc., it has been applied to develop protective products used in aerospace, high-temperature environments and civil fields [32,33]. The electrospun PSA nanofibers not only have nanostructure but also preserved the superior properties, such as crystallization, thermal performance and mechanical properties [34]. However, there is no research about PSA/G nanocomposite has been reported. The field of potential applications of graphene-polymer nanocomposite could be tremendously expanded by developing PSA/G nanocomposites with improved thermal and electrical properties, such as electrodes and separators, batteries and supercapacitors.

For the electronic components applications, the electrospun fiber mats are capable of improving battery power, increasing energy density of capacitors, and fuel cell and solar cell efficiency [35-37]. The electrospun fiber mats are widely used as commercial separator for Li-ion batteries. Only the mats with perfect performance can meet the necessary of application. The uneven thickness of separator will influence on the impedance properties and the distribution of current densities, which will reduce the properties of Li-ion batteries. Therefore, a electrospinning system was employed for the PSA/G nanocomposite fabrication, in order to obtain membranes with uniform thickness in the paper.

We present the fabrication of the PSA/G nanocomposite using electrospinning technique in this study. Five PSA/G composites with different graphene concentrations (i.e., 0.1 %, 0.3 %, 0.5 %, 0.7 %, 0.9 %) were prepared to investigate the effects of graphene on the thermal and electrical properties. Meanwhile, the neat PSA nanofiber mat also prepared as a control standard reference. Furthermore, three-dimensional

*Corresponding author: yuansheng@sues.edu.cn
*Corresponding author: xinbj@sues.edu.cn

electric field of the electrospinning system was simulated with finite element method (FEM) to understand the effects of electric field distribution on the thickness of PSA/G nanocomposites.

Experimental

Materials and Chemicals

The PSA ($C_{20}H_{14}O_4N_2S$, degree of polymerization ⩾ 396, average molecular weight is 150000-200000, 12 wt%, Shanghai Tanlon Fiber Co., Ltd., China) and *N*,*N*-dimethyl-acetamide (DMAc, analytical grade, $CH_3CON(CH_3)_2$, molecular weight is 87.12, Sinopharm Chemical Reagent Co., Ltd., China) was used as received. Graphene powder (<20 μm, Xinhe New Materials Co., Ltd., China) was used as received.

PSA/G Solution Preparation

The preparation process of the PSA/G solution was shown in Figure 1. A certain amount of graphene was dispersed in the DMAC solution using ultrasonic vibration by using a bath for 30 min at 40. The PSA/G solution was prepared by adding the mixture solution of graphene and DMAC into 12 wt% PSA solution solubilized with DMAC under continuous stirring for 10 hours at the room temperature. Detailed description of the mixing of graphene in electrospinning solutions were illustrated in Table 1.

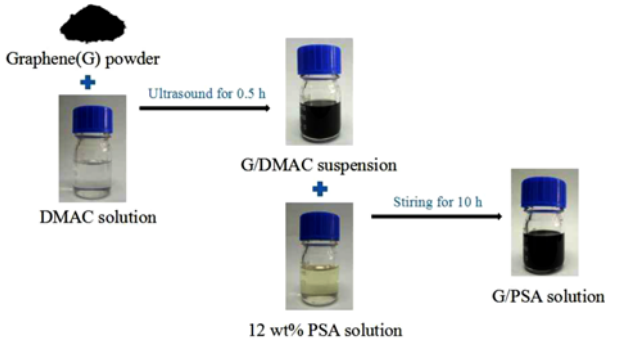

Figure 1. The preparation process of the PSA/G solution.

Table 1. Different concentrations of graphene (G) in the PSA solutions

Graphene concentration (%)	12 wt% PSA solution (g)	Graphene (mg)	DMAC (g)
0	40	0	8
0.1	40	4.8	7.9952
0.3	40	14.4	7.9856
0.5	40	24.0	7.9760
0.7	40	33.6	7.9664
0.9	40	43.2	7.9568

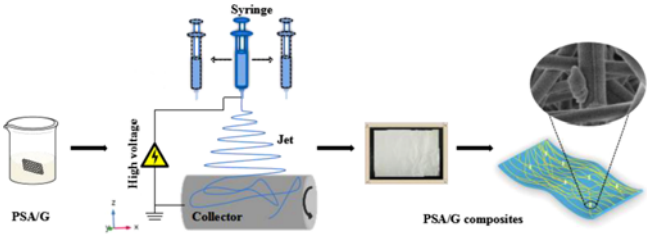

Figure 2. Schematic illustration of the fabrication of PSA/graphene nanocomposites by dynamic electrospinning system.

PSA/G Composites Fabrication

The schematic illustration of the fabrication of PSA/graphene nanocomposites by dynamic electrospinning system used in this study is shown in Figure 2. The dynamic electrospinning system includes a dynamic spinneret, a high voltage power supply, and a rotating roller collector. The dynamic spinneret consists of a needle and a 3-mm thick plastic plate made of polytetrafluoroethylene (PTFE) (no shown in Figure 2). Needle was fixed with the PTFE plate, and a motor drives the PTFE plate moving left and right during the electrospinning process. The stainless-steel needle was blunt-tip type with an outer diameter of 0.9 mm, inner diameter of 0.6 mm, and length of 13 mm. The PSA/G solution was extruded from a syringe via a propulsion module through a 2-mm inner diameter plastic pipe to a 2-mm outer diameter plastic pipe inlet to supply solution for the spinning. An extruding speed of spinning solution used is set to be 1.5 m*l*/h. The high voltage power supply (RS60P-20 W, Gamma High Voltage Research, USA) with operating voltage ranging from 0 to 50 kV, and 30 kV was applied to the spinneret and the collector in this study. The distance between the needle and the receiver was set to be 10 cm. An aluminum roller receiver with a certain rotating speed was employed to collect the electrospun PSA/G nanocomposites. All the electrospinning experiments were conducted under the condition of 25 °C 60±5 % RH of humidity.

Characterization

SEM

The morphology of PSA/G composites was observed under a scanning electron microscope (SEM) (SU8010, Hitachi, Japan) with an accelerated voltage of 2 kV. The surfaces of the samples were coated with a sputter coater (S450, Hitachi, Japan) equipped with a gold target to increase electrical conductivity of the samples. The fiber diameters typically are measured from images obtained from a scanning electron microscope (SEM) by using the ImageJ software. Fiber diameters are selected 50 random fibers to achieve testing, and are reported by a mean value (average value) with the standard deviation (a measure of variability).

FTIR Analysis

Tests on chemical composition and molecular structure of the PSA/G composite were performed by the Spectrum-two

FTIR (Spectrum Two, Perkin Elmer, USA) under the circumstances: attenuated total reflection, scanning times for 16, data interval of 2 cm^{-1}, resolution ratio of 16 cm^{-1}, sample dimensions of 1 cm×1 cm.

Volume Resistivity Analysis

The electrical properties were measured using KEYSIGHT 34461A Dight Multimeter. The test conditions were configured with a clamping length of 10 mm, drawing speed is 10 mm/min and the pre-tensioning force of 0.1 cN. Each sample was measured five times, and then the arithmetic mean was calculated.

TGA Analysis

The thermal stability of PSA/G composites were characterized by thermal gravimetric analyzer (TGA) using a TGA-4000 thermal gravimetric analyzer (TGA4000, Perkin Elmer, USA). The TGA experiment was carried out in a nitrogen atmosphere with a gas flow of 19.8 m*l*/min. The samples, with a weight of 5-8 mg, were heated from room temperature to 700 °C at a heating rate 10 °C/min under a nitrogen atmosphere. Five samples for each group were measured.

Fiber Mats Thickness

A micrometer is used to measure the thickness of nanocomposites mat. The thickness was measured every 1 cm along the roller axis.

Results and Discussion

Morphology

The electron microscopy images of the graphene sheets are shown in Figure 3, which confirm the layer-like morphology of the graphene powder. Figure 4 shows the representative SEM images of the electrospun nanocomposites from PSA/G solution and neat PSA solution. The SEM images of neat PSA are depicted in Figure 4(a) to (c) for comparison. As illustrated in Figure 4(a), the electrospun PSA fibers form a highly interconnected mat, the surfaces of fibers are relatively smooth and the fibers are randomly oriented. However, due to jet instabilities, some coarse fiber

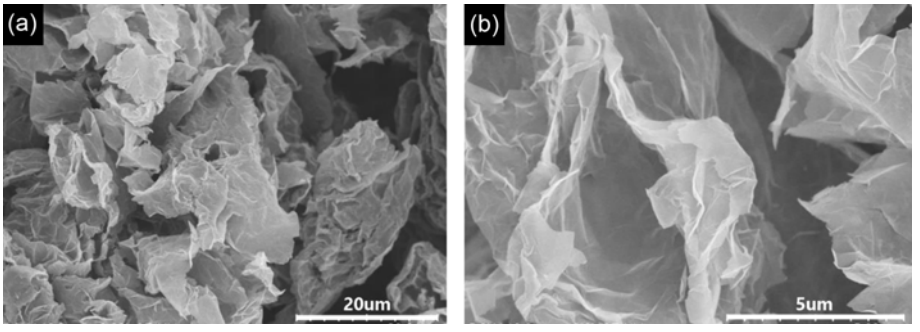

Figure 3. SEM image of graphene; (a) 2000 times magnification and (b) 5000 times magnification.

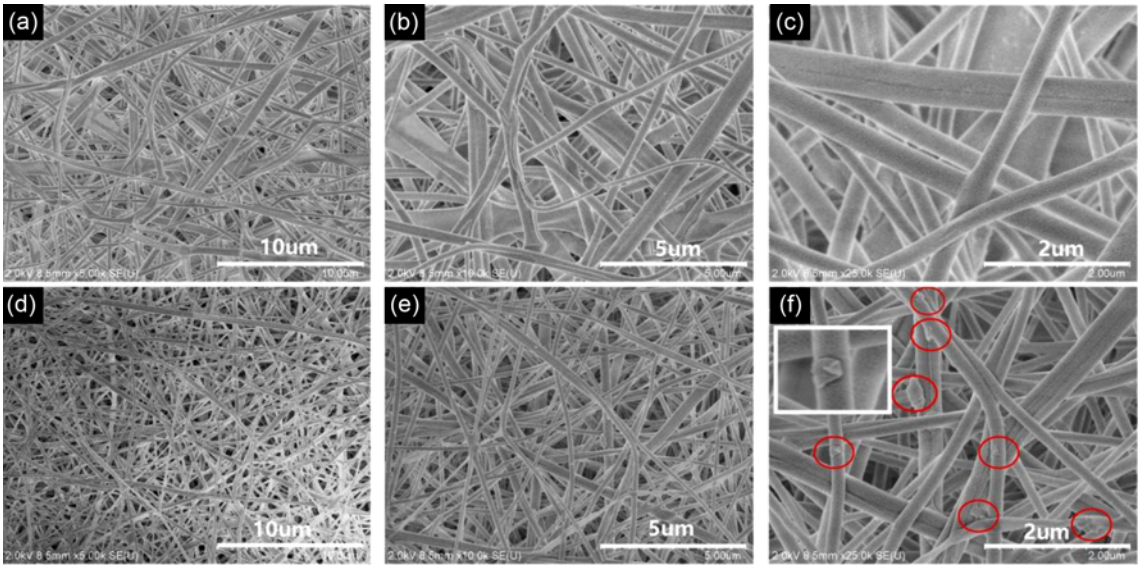

Figure 4. (a-c) SEM images of PSA nanofibers at different magnification, (d-f) SEM images of 0.7 % P SA/G nanofibers at different magnification.

can be observed in Figure 4(a) to (c). The same characteristics were observed for PSA/G nanofibers, Figure 4(d) to (f). It can be seen from Figure 4(f) that the graphene dispersed on the surface of fiber mat in the form of particles or sheet. From the magnified graphene particles, it could be found that most of the particles graphene are aggregated. Meanwhile, we also found that graphene reunion phenomenon more obvious with the addition of graphene, indicating that graphene powders are hardly to be uniformly dispersed after mixing with PSA solution by high speed stirring and ultrasonicating. The existential form of graphene in PSA/G composites is adhered to the nanofiber surface instead of dispersion within the PSA. The main reason was that the size of the graphene sheet (as shown in Figure 4) is rather large compared with the diameter of nanofibers (150-450 nm), the graphene nanosheet is unlikely in the inner part of the nanofibers. Therefore, we can conclude that graphene powders are dispersed on the surface of composites fiber mat in the form of particles.

The average diameter of nanofibers is calculated from SEM and shown in Figure 5. The average diameter of nanofibers with and without graphene basically decreased with increasing the concentration of graphene. The fiber diameter distribution for PSA nanofibers lies in the range of 150-450 nm with an average diameter of 300 nm, whereas for 0.7 % PSA/G nanofibers the fiber diameters are in the range of 100-200 nm with an average diameter of 150 nm. The standard deviation of the nanofibers also decreased with the increasing of graphene as shown in Figure 5. This decrease in the average diameter and standard deviation of PSA nanofibers in comparison to PSA/G nanofibers can be attributed to the presence of graphene sheets in the fibers, which give rise to the increased electrical conductivity, which probably help to reduce the jet instability in electrospinning process.

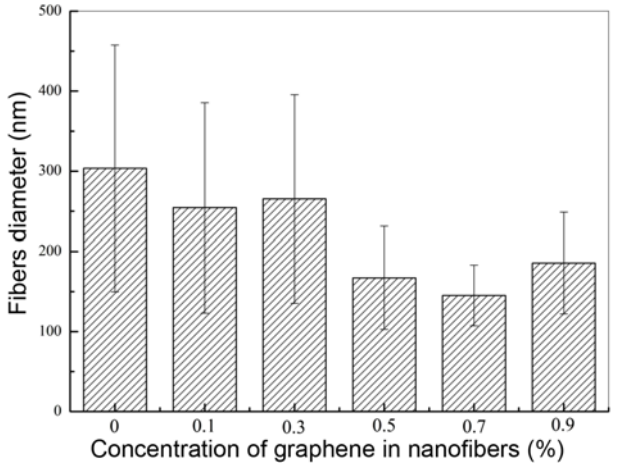

Figure 5. The diameter of nanofiber with various concentration of graphene. The length of the error bar represents the standard deviations of the fiber diameter.

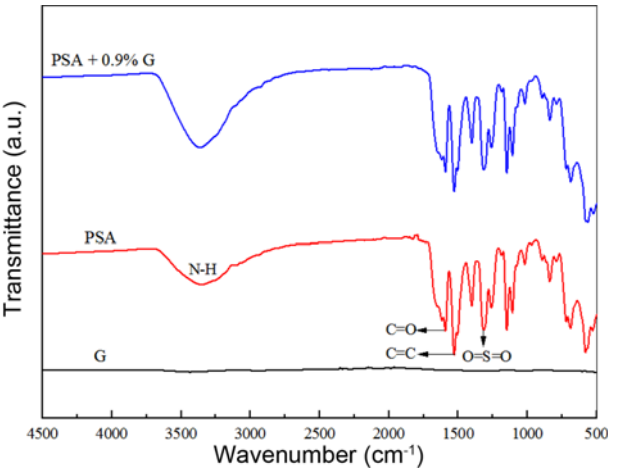

Figure 6. FTIR spectra of graphene (G), PSA and 0.9 % PSA/G.

Chemical Structural

Fourier transform infrared (FTIR) spectroscopy was performed on the graphene powder, PSA nanofiber mats and PSA/G nanocomposite in order to verify the presence of fingerprint of functional groups of the graphene nanosheets. As shown in Figure 6, no peaks shown in the spectra of G, and the spectrum of 0.9 % PSA/G do not have much difference with that of pure PSA, which provide the evident of the purity of the graphene powder. In the spectrum of PSA and PSA/G the presence of vibration peaks at 3362 cm^{-1} which is due to the stretching vibration of N-H. The symmetric and antisymmetric stretching vibration absorptions of sulfone -SO_2 were at 1305 cm^{-1}. Moreover, the peaks at 1656 cm^{-1} and 1589 cm^{-1} correspond to the out-of-plane vibration of the C=O and C=C stretching vibration, respectively. In addition, the opposite-substituted peak of benzene appeared at 834 cm^{-1}, and thus the exiting of PSA could be determined [38].

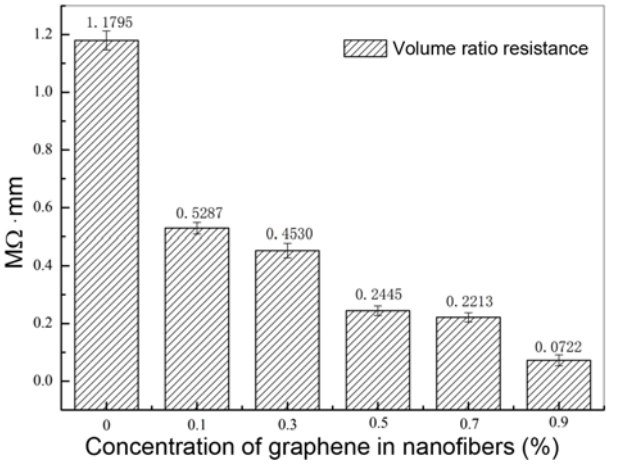

Figure 7. Volume resistivity of PSA nanofibers with and without graphene at different compositions.

Electrical Properties

Volume ratio resistance of the as-prepared PSA and PSA/G nanofiber mat with relatively same thickness (~190 μm) was measured using digital multimeter at room temperature. The volume ratio resistance results were illustrated in Figure 7. The volume ratio for PSA nanofiber mat was 1.1795 MΩ·mm, and the volume ratio for PSA/G nanocomposite decrease from 0.5287 MΩ·mm to 0.0722 MΩ·mm. The value of volume ratio resistance is a sharp decrease due to the addition of graphene, indicating that the addition of graphene could enhance the electrical properties of polysulfone amide. As can be seen 0.9 % PSA/G showed about 16 times higher conductivity in comparison to PSA.

Thermal Stability

Thermal stability of electrospun PSA and PSA/G nanofiber mats and bulk G were measured using TGA in nitrogen atmosphere. The TG and TGA curves of graphene, PSA and the PSA/G composites are illustrated in Figure 8. From the TG curve (Figure 8(a)), it can be observed that pure PSA can be divided into roughly four intervals [39]. The first stage is in the range of 95-105 °C, which comes mainly from the volatilization of combined water between polymer molecules and various additives when room temperature is up to 100 °C. The second phase is 200-300 °C, there is suppressed (and shifted at higher temperature) by adding graphene around 240 °C. The third is 400-500 °C, which loss may be the increasing high-polymer macromolecule chain movement rate until fracture, with small molecular substances releasing in the form of gas formation. The fourth is carbon stable stage (600-700 °C). There is not much effect of weightlessness when rising temperature as a result of that most polymer materials have carbide [40]. When graphene was added to the PSA, the residual rates of the nanocomposites were larger than that of pure PSA, as shown in Figure 8(b). Moreover, with addition of the graphene, the temperature of the third stage is higher than pure PSA. This shows that the incorporation of small amount of graphene in PSA improve its thermal stability, which can be attributed to the presence of interfacial bonding.

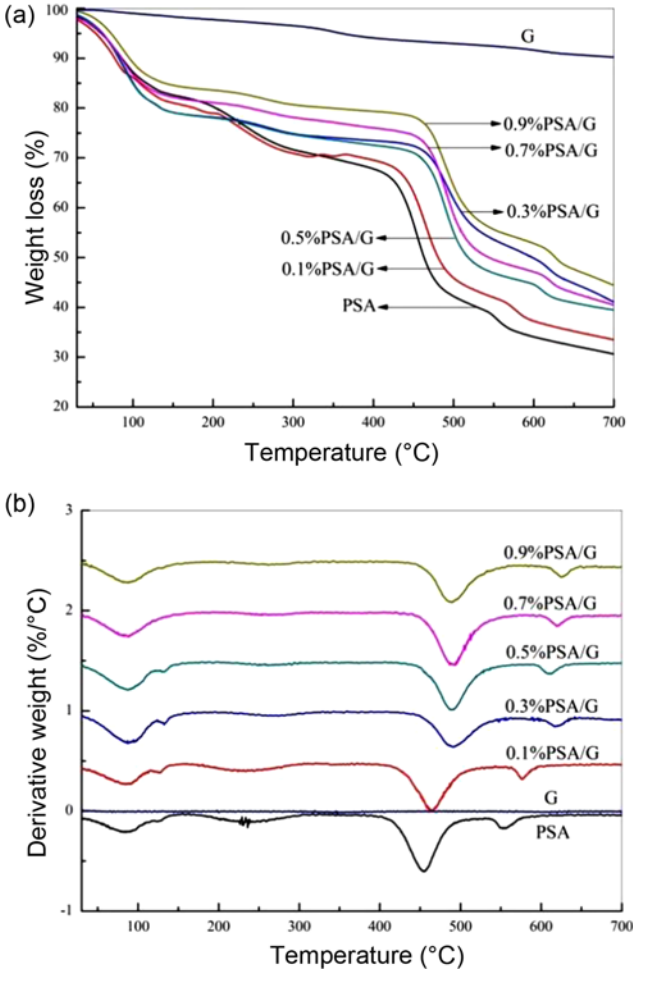

Figure 8. TG curves (a) and the DTG curves (b) of PSA nanofibers with and without graphene at different compositions.

Thickness of the Nanocomposites Mats

The thickness uniformity of the electrospun nanocomposites is rather important in practical applications. The uneven thickness of separator will influence on the impedance properties and the distribution of current densities for the batteries application. The thickness uniformity of the electrospun PSA/G nanocomposite was investigated by measuring the thickness of nanocomposites along the axis direction of the collector after spinning for 180 min. In this study, the thickness was measured by five points (i.e., x=0, x=50, x=100, x=150, x=200) along x-axis direction (graphene concentration 0.5 %). As presented in Figure 9, rather uniform composite fiber mat was obtained by using the dynamic electrospinning system, even at the edge of the mats. As we all know, the electrospun fiber mat was thick in

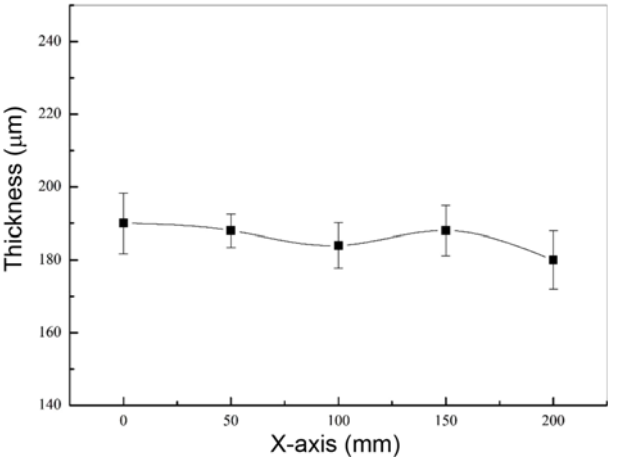

Figure 9. The thickness of the fiber web after 180 min spinning.

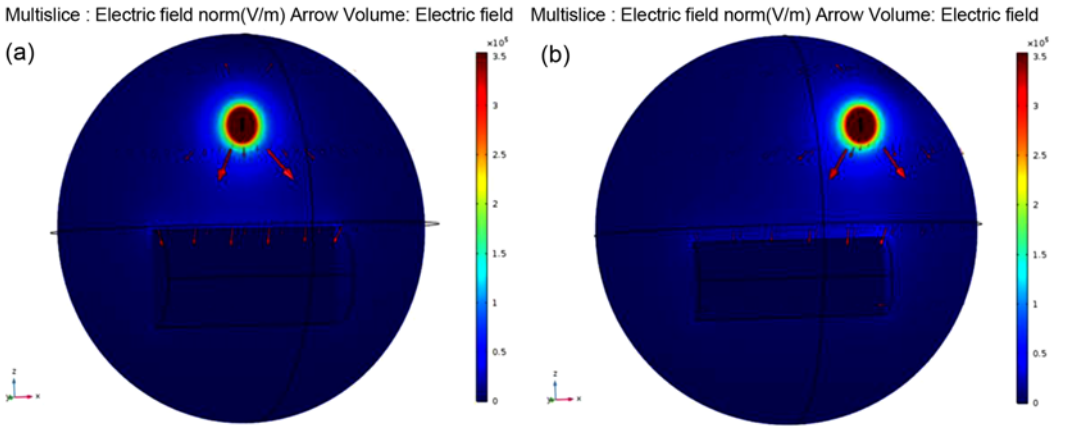

Figure 10. The electric field distributions for the dynamic electrospinning system with a working distance of 10 cm and an applied voltage of 30 kV when the needle at two difference positions; (a) at the central position of the collector and (b) at the edge position of the collector.

the middle position because of the jet whipping and instability, and the thickness uniformity can be improved by designing the electric distribution of the electrospinning system [41,42]. To understand the effect of electric field distribution on the fiber mats thickness, the 3D electric fields of the dynamic electrospinning system were analyzed by COMSOL Multiphysics® software using the finite element method (FEM). Before the simulation, the physical geometries of the electrospinning setups (e.g., needle and collector) were established and set according to their practical dimensions and locations.

Figure 10 shows the electric field distributions of the dynamic electrospinning system when the needle at two different positions. The arrows indicate the direction of the electric field, and their length is proportional to the strength at that position. As shown in Figure 10(a), the electric field distribution is symmetrical along the needle when the needle at the central position of the roller collector, the electric field intensity at central position is higher than that at two side positions. When the needle moved to the edge side of the collector, the electric field at the other side is much smaller than that at the needle side. The edge of the collector has an aggregation effect to electric field, the arrows representing the direction of the electric field is converging toward the edge of the roller as shown in Figure 10(b). Regardless of the needle in anywhere, there is a sharp decrease of electric field intensity from the spinneret to the collector. The fiber mat electrospun by electrospinning will be thicker at the central part than that at edge part when the needle at the central position because of the whipping of the jet. When the needle is moved to the edge side, the edge of the roller will help to collect and assemble the fibers due to the higher electric field intensity of the collector edge. Thus, in this dynamic electrospinning system, the movement of the needle along roller collector will help to achieve a more uniform fiber mat.

Conclusion

In conclusion, we have demonstrated that the addition of graphene can improve the thermal and electrical properties of poly(sulfone amide) through the preparation of PSA/G nanocomposites via a dynamic electrospinning system. Three-dimensional electric field of the electrospinning system was simulated with finite element method (FEM), it reveals that the electric field distribution can affect the thickness of PSA/G nanocomposites, swinging the needle along the roller collector in the electrospinning can obtain more uniform PSA/G nanocomposites. With significant thermal and electrical prosperity and uniform thickness, the PSA/G nanocomposite mat can be effectively applied in electric component industrial fields.

Acknowledgment

The authors disclosed receipt of the following financial support for the research, authorship, and/or publication of this article: This work was supported by the National Natural Science Foundation of China (Grant No. 11702169), Scientific Research Staring Foundation of Shanghai University of Engineering Science (Grant No. 2017-19), and Talents Action Program of Shanghai University of Engineering Science (Grant No. 2017RC522017) to Dr. Y. Zheng. This work was also supported by Talents Action Program of Shanghai University of Engineering Science (Grant No. 2017RC432017) to Dr. B. Xin and Graduate Research Projects for the Shanghai University of Engineering Science (Grant No. 17KY0906) to N. Meng.

References

1. L. Persano, A. Camposeo, C. Tekmen, and D. Pisignano, *Macromol. Mater. Eng.*, **298**, 504 (2013).

2. X. X. He, J. Zheng, and G. F. Yu, *J. Phys. Chem. C.*, **121**, 8663 (2017).
3. L. F. Zhang, A. Aboagye, and A. Kelkar, *J. Mater. Sci.*, **49**, 463 (2014).
4. X. Wang, J. Yu, G. Sun, and B. Ding, *Mater. Today*, **19**, 403 (2015).
5. J. F. Kim, J. H. Kim, Y. M. Lee, and E. Drioli, *Aiche J.,* **62**, 461 (2016).
6. M. Mirjalili and S. Zohoori, *J. Nanostruct. Chem*., **6**, 1 (2016).
7. H. R. Shan, J. Y. Yu, and B. Ding, *ACS Appl. Mater. Inter.*, **9**, 1 (2017).
8. X. L. Zhao, Y. Y. Li, T. Hua, P. Jiang, X. Yin, J. Y. Yu, and B. Ding, *Acs Appl. Mater. Inter.*, **9**, 12054 (2017).
9. X. Wang, B. Ding, and B. Li, *Mater. Today*, **16**, 229 (2013).
10. L. Jin, T. Wang, M. L. Zhu, M. K. Leach, Y. I. Naim, J. M. Corey, Z. Q. Feng, and Q. Jiang, *J. Biomed. Nano Technol.*, **8**, 1 (2012).
11. Y. F. Goh, I. Shakir, and R. Hussain, *J. Mater. Sci.*, **48**, 3027 (2013).
12. C. Ball, S. F. Cho, Y. Jiang, and K. A. Woodrow, *Mater. Sci. Eng. C*, **63**, 117 (2016).
13. A. Luzio, E. Canesi, C. Bertarelli, and M. Caironi, *Materials*, **7**, 906 (2014).
14. S. N. Raja, A. C. K. Olson, K. Thorkelsson, A. J. Luong, L. Hsueh, G. Q. Chang, B. Gludovatz, L. W. Lin, T. Xu, R. O. Ritchie, and A. P. Alivisatos, *Nano Lett.*, **13**, 5762 (2013).
15. S. Homaeigohar and M. Elbahri, *Materials*, **7**, 1017 (2014).
16. A. J. Hassiba, M. E. Zowalaty, T. J. Webster, A. M. Abdullah, G. K. Nasrallah, K. A. Khalil, A. S. Luyt, and A. A. Elzatahry, *Int. J. Nano Med.*, **12**, 2205 (2017).
17. X. F. Wang, B. Ding, J. Y. Yu, and M. R. Wang, *Nano Today*, **6**, 510 (2011).
18. H. Fashandi, M. M. Abolhasani, P. Sandoghdar, Z. Nima, Q. X. Li, and N. Minoo, *Cellulose*, **23**, 1 (2016).
19. S. Panzavolta, B. Bracci, C. Gualandi, M. L. Focarete, E. Treossi, K. K. Agalou, K. Rubini, F. Bosia, L. Brely, N. M. Pugno, V. Palermo, and A. Bigi, *Carbon*, **78**, 566 (2014).
20. F. Navarro-Pardoa, A. L. Martinez-Hernandeza, and C. Velasco-Santosa, *J. Nano Mater.*, **2016**, 1 (2016).
21. Z. Xu and C. Gao, *Mater. Today*, **18**, 480 (2015).
22. C. Lee, X. Wei, J. W. Kysar, and J. Hone, *Science*, **321**, 385 (2008).
23. T. T. Dang, V. H. Pham, S. H. Hur, E. J. Kima, B. S. Kongb, and J. S. Chung, *J. Coll. Interface. Sci.*, **376**, 91 (2012).
24. W. Tong, G. L. Luo, Z. J. Fan, C Zheng, J. Yan, C. Z. Yao,W. F. Li, and C. Zhang, *Carbon*, **47**, 2296 (2009).
25. H. Gu, Y. Huang, L. Zuo, W. Fan, and T. X. Liu, *Electrochim. Acta*, **219**, 604 (2016).
26. H. Quan, B. Q. Zhang, Q. Zhao, R. K. K. Yuen, and R. K. Y. Li, *Compos. Pt. A-Appl. Sci. Manuf.*, **40**, 1506 (2009).
27. G. Eda and M. Chhowalla, *Nano Lett.*, **9**, 814 (2009).
28. J. Liang, Y. Xu, Y. Huang, L. Zhang, Y. Wang, Y. F. Ma, F. F. Li, T. Y. Guo, and Y. S. Chen, *J. Phys. Chem. C*, **113**, 9921 (2009).
29. H. Kim and C. W. Macosko, *Polymer*, **50**, 3797 (2009).
30. T. Ramanathan, A. A. Abdala, S. Stankovich, D. A. Dikin, M. Herrera-Alonso, R. D. Piner, D. H. Adamson, H. C. Schniepp, X. Chen, R. S. Ruoff, S. T. Nguyen, I. A. Aksay, R. K. Prud'homme, and L. C. Brinson, *Nat. Nano Technol*., **3**, 327 (2008).
31. S. Stankovich, D. A. Dikin, G. H. B. Dommett, K. M. Kohlhaas, E. J. Zimney, E. A. Stach, R. D. Piner, S. T. Nguyen, and R. S. Ruoff, *Nature*, **442**, 282 (2006).
32. Z. M. Chen, B. J. Xin, X. J. Wu, X. F. Wang, and W. P. Du, *Fibres Text. East Eur.*, **94**, 21 (2012).
33. J. L. Yu, B. J. Xin, and C. C. Shen, *Text. Res. J.*, **87**, 528 (2016).
34. W. J. Chen, B. J. Xin, and X. J. Wu, *J. Ind. Text.*, **44**, 159 (2014).
35. F. Pierini, M. Lanzi, P. Nakielski, S. Pawłowska, K. Zembrzycki, and T. A. Kowalewski, *Polym. Advan. Technol.*, **27**, 1465 (2016).
36. R. Sood, S. Cavaliere, D. J. Jones, and J. Rozière, *Nano Energy*, **26**, 729 (2016).
37. F. Pierini, M. Lanzi, P. Nakielski, S. Pawłowska, O. Urbanek, K. Zembrzycki, and T. Kowalewski, *Macromolecules*, **50**, 4972 (2017).
38. W. J. Chen, B. J. Xin, X. J. Wu, X. F. Wang, and W. P. Du, *Technol. Text.*, **7**, 7 (2013).
39. B. J. Xin, Z. M. Chen, X. J. Wu, and X. F. Wang, *J. Ind. Text.*, **42**, 434 (2013).
40. T. Xi and B. J. Xin, *J. Ind. Text.*, 1 (2016).
41. C. R. Yang, Z. D. Jia, J. N. Liu, Z. H. Xu, Z. C. Guan, and L. M. Wang, *IEEE Transactions on Dielectrics & Electrical Insulation,* **16**, 785 (2009).
42. Y. S. Zheng, X. K. Liu, and Y. C. Zeng, *J. Appl. Polym. Sci.*, **130**, 3221 (2014).